

1 Microlite transfer by disaggregation of mafic inclusions following magma
2 mixing at Soufrière Hills Volcano, Montserrat

3
4 Madeleine C.S. Humphreys*¹, Thomas Christopher² & Vicky Hards²†

5
6 * Corresponding author

7 ¹Department of Earth Sciences, University of Cambridge, Downing Street, Cambridge, CB2 3EQ, UK. Tel: +44
8 (0)1223 333433; Fax: +44 (0)1223 333450; mcsh2@cam.ac.uk

9 ²Montserrat Volcano Observatory, Flemings, Montserrat, West Indies

10 † Current address: British Geological Survey, Keyworth, Nottingham, NG12 5GG

11
12
13 **ABSTRACT**

14 The Soufrière Hills Volcano on Montserrat has for the past twelve years been erupting
15 andesite with basaltic to basaltic-andesite inclusions. The andesite contains a wide variety of
16 phenocryst textures and strongly zoned microlites. Analysis of minor elements in both
17 phenocrysts and microlites allows us to put detailed constraints on their origins. Compositions
18 of clinopyroxene, from overgrowth rims on quartz and orthopyroxene and coarse-grained
19 breakdown rims on hornblende, are identical to those from the mafic inclusions, indicating
20 that these rims form during interaction with mafic magma. In contrast, resorbed quartz and
21 reversely zoned orthopyroxenes form during heating. Microlites of plagioclase and
22 orthopyroxene are chemically distinct from the phenocrysts, being enriched in Fe and Mg,
23 and Al and Ca respectively. However, microlites of plagioclase, orthopyroxene and
24 clinopyroxene are indistinguishable from the compositions of these phases in the mafic
25 inclusions. We infer that the inclusions disaggregated under conditions of high shear stress
26 during ascent in the conduit, transferring mafic material into the andesite groundmass. The
27 mafic component of the system is therefore greater than previously thought. The presence of
28 mafic-derived microlites in the andesite groundmass also means that care must be taken when
29 using this as a starting material for phase equilibrium experiments.

30
31
32 **Keywords:** magma mixing, mafic inclusions, microlites, hybridisation, disaggregation;
33 Soufrière Hills volcano; Montserrat

35 **INTRODUCTION**

36 Magma mingling (incomplete mixing, resulting in macroscopic enclaves or compositional
37 banding) and mixing or hybridisation (complete mixing) have long been recognised at
38 intermediate arc volcanoes (e.g. Anderson 1976; Eichelberger 1980; Bacon 1986; Feeley &
39 Dungan 1996; Clynne 1999). Mixing tends to occur between a relatively silicic resident
40 magma and a more mafic replenishing magma (typically basalt to basaltic andesite).
41 Petrological characteristics indicating mixing span a wide range of scales, from macroscopic
42 mafic inclusions and compositional banding, to partially reacted xenocrysts or strongly zoned
43 phenocrysts (e.g. Eichelberger 1978, Clynne 1999).

44
45 The degree of interaction between the resident silicic magma and the replenishing magma
46 depends strongly on the relative viscosities, temperatures, compositions and volumes of the
47 two end-members (Sparks & Marshall 1986). For example, if the volume proportion of silicic
48 magma is relatively large, significant mixing can only take place with a relatively evolved
49 incoming magma. For significant mixing to occur with a more mafic incoming magma, the
50 volume proportion of the mafic component must be large (Sparks & Marshall 1986). The
51 presence of mafic inclusions indicates rapid quenching of the mafic magma against the cooler
52 silicic host, and suggests only limited contact between the two end-members. However, a
53 recent study suggested that plagioclase microlites were transferred from basaltic andesite to
54 andesite during mixing at Mont Pelée volcano, Martinique (Martel et al.2006), suggesting a
55 more intricate interaction. Evaluating the extent, timing and nature of such mixing is
56 important because it will affect the viscosity, and thus the ascent and eruption of magma
57 (Melnik & Sparks 1999).

58
59 This study will address the nature and mechanism of magma mingling and hybridisation at
60 Soufrière Hills Volcano, Montserrat. Mixing between the host andesite and incoming basaltic
61 to basaltic-andesite magma initially formed quenched magmatic inclusions. We present
62 evidence that substantial quantities of plagioclase, orthopyroxene, clinopyroxene and
63 titanomagnetite microlites were later transferred from basaltic andesite inclusions into the
64 host andesite. We discuss possible mechanisms for the transfer of material and the effects on
65 viscosity and temperature.

66
67

68 **SAMPLES AND METHODS**

69 The 14 samples studied include 13 samples of andesite and one macroscopic mafic inclusion
70 (table 1). The samples were deposited between July 2001 and May 2006 and represent dome
71 and pyroclastic flow material. Modal analysis was done by point-counting approximately
72 1500-2000 points in every thin section, with a spacing of ~0.5 mm. Vesicles were counted
73 separately from the groundmass where possible.

74
75 Electron micro-probe analyses were carried out using a Cameca 5-spectrometer SX-100
76 instrument. Minerals were analysed using a 2 µm, 15 kV, 10 nA beam for major elements and
77 a 100 nA beam for minor and trace elements. Structural formulae were recalculated on the
78 basis of 23 O atoms for hornblende (Schumacher 1997) and using Stormer (1983) for oxide
79 minerals.

80

81 **ANDESITE PETROLOGY**

82 The samples are crystal rich (typically 35-40 vol% phenocrysts, table 2) and similar to
83 previously described samples from earlier in the eruptive episode (e.g. Devine et al.1998;
84 Barclay et al.1998; Murphy et al.2000; Couch et al.2001). In this study, the term ‘phenocryst’

85 is used for large crystals, regardless of their origin (c.f. Davidson et al. 2007); ‘microlite’ is
86 used for crystals smaller than ~100 µm, and ‘microphenocryst’ is used for crystals
87 approximately 100-300 µm, following Murphy et al. (2000). In the andesite, the phenocryst
88 assemblage is plagioclase + hornblende + orthopyroxene + Fe-Ti oxides, with minor apatite,
89 quartz and clinopyroxene, and rare zircon. The groundmass comprises plagioclase +
90 orthopyroxene + clinopyroxene + Fe-Ti oxides + rhyolitic glass. In some samples, the glass is
91 partly devitrified or has undergone phase separation to patches of glass enriched in Ca+Na
92 and patches enriched in K+Fe (Cashman, 1992). Quartz is present in the groundmass of some
93 samples, where it can act as a nucleation point for intergrowths of feldspar and quartz.
94 Vesicles are commonly partially filled with cristobalite. Plagioclase microlites may have
95 calcic cores overgrown by more sodic material. In some samples, two populations of
96 microlites are observed, with a population of small, skeletal crystals inferred to have formed
97 during a second nucleation event.

98

99 **Andesite phenocryst textures**

100 Plagioclase crystals show varied textures, including oscillatory zoning, sieve textures and
101 patchy cores. Quartz is present in all samples, but is resorbed and embayed or overgrown by
102 clinopyroxene. Clinopyroxene occurs as single crystals or clusters of oscillatory- and sector-
103 zoned microphenocrysts. Hornblende phenocrysts are typically euhedral and variably replaced
104 by ‘opacite’, a very fine-grained aggregate of Fe-Ti oxides and pyroxene (Garcia & Jacobson
105 1979; Murphy et al. 2000; Plechov et al. 2008a). Replacement by opacite (figure 1a) initiates
106 preferentially adjacent to vesicles, suggesting an origin in the circulation of oxidising fluids
107 during shallow storage, and implying high permeability. Hornblende phenocrysts may show
108 oscillatory zoning or distinct zoned rims. They commonly have a breakdown rim due to
109 decompression (figure 1a; Rutherford & Hill 1993; Rutherford & Devine 2003; Buckley et al.
110 2006); the width of the rim varies from a few microns to several hundred microns. Almost all
111 samples also contain a minority of hornblende phenocrysts with thick, cpx-rich, thermal
112 reaction rims (Rutherford & Devine 2003) of plagioclase + pyroxene (aligned parallel to the
113 c-axis of the amphibole grain) + oxides + glass (figure 1b). These result from heating the
114 amphibole above its thermal stability limit, which is thought to be ~ 880 °C (Barclay et al.
115 1998). In these phenocrysts, any included plagioclase are commonly sieved and any
116 orthopyroxene inclusions have Mg-rich rims or clinopyroxene overgrowths. Orthopyroxene
117 phenocrysts are euhedral and may have Mg-rich rims or, less commonly, overgrowths of
118 clinopyroxene. These are interpreted as indicators of heating (Rutherford & Devine 2003).
119 Some of the reversely zoned rims comprise two distinct zones of Mg-enrichment (figure 1c)
120 followed by normal zoning, suggesting multiple episodes of heating.

121

122 **Mafic inclusions**

123 The andesite contains macroscopic mafic inclusions as observed in previous stages of the
124 eruption (Murphy et al. 2000). The mafic inclusions are vesicular, with interstitial rhyolitic
125 glass, and occur in all sizes, down to mm-sized inclusions. The vesicles typically inhabit
126 voids between crystals (figure 1d,e), suggesting that vesiculation was induced by
127 crystallisation (Browne et al. 2006; Martin et al. 2006). They typically contain elongate,
128 randomly oriented crystals (figure 1d) of An-rich plagioclase + clinopyroxene ±
129 orthopyroxene. Fe-Ti oxides are abundant, and yellowish, subhedral amphibole is common.
130 Ilmenite is more common than it is in the andesite. Amphibole is dominant in larger
131 inclusions, whereas pyroxene dominates in smaller inclusions (Murphy et al. 2000). This
132 variation in mineral assemblage may be related to variations in degree of undercooling for
133 different sizes of inclusion (Blundy & Sparks 1992) or to slight differences in composition of
134 the incoming magmas. Large, sieve-textured plagioclase and clear plagioclase phenocrysts are

135 also seen, together with euhedral clinopyroxene and rare olivine (Fo₇₅) microphenocrysts.
136 Large hornblende crystals are present, but always show a thermal reaction rim, and the larger
137 feldspars are usually sieved (see above). Similarly, orthopyroxene phenocrysts are also
138 present, but show reverse-zoned rims or clinopyroxene overgrowths. These hornblende, large
139 sieve-textured plagioclase and orthopyroxene crystals are interpreted from their textural
140 characteristics as xenocrysts that originated in the andesite.

141
142 ‘Crystal cluster’ is used here to describe material, found in the andesite, that is similar to the
143 mafic inclusions in terms of mineralogy and texture, but typically comprises only a few grains
144 together with glass ± microlites (figure 1e). Yellowish amphibole is common in these small
145 crystal clusters. In some cases, amphibole may be overgrown by clinopyroxene.

146 147 **Crystal clots**

148 Crystal clots are texturally distinct from the mafic inclusions and crystal clusters. Clots
149 typically comprise euhedral, equant grains of orthopyroxene + Fe-Ti oxides + apatite ±
150 plagioclase (figure 1f) + clear glass. Apatite is clear to brownish; the brown colour apparently
151 results in part from lots of tiny, oriented inclusions of an opaque mineral. Euhedral zircon
152 grains are also found. Some of the crystal clots show evidence of having been recently heated,
153 in that the plagioclase grains are sieve-textured and there is reverse zoning in the
154 orthopyroxene.

155 156 157 **GEOCHEMISTRY OF PHENOCRYSTS, MICROLITES AND MAFIC MATERIAL**

158 **Plagioclase**

159 Plagioclase compositions span a wide range, from An₃₁ to An₉₅ (table 3). Crystals with
160 different textures show clear compositional differences (figure 2). Most phenocryst analyses
161 lie between An₄₅ and An₈₀, and show a slight positive correlation with FeO content. However,
162 some phenocryst analyses, typically from traverses which cross narrow sieve zones or
163 resorption surfaces, follow a curved trend at higher FeO (figure 2). The same trend is
164 followed by the rims of sieve-textured plagioclase, while the cores have compositions that are
165 indistinguishable from other phenocrysts (An₄₅-An₈₀ and “normal” FeO). Material just outside
166 the sieved zone is very calcic, up to An₉₁, and becomes more sodic with increasing FeO. The
167 outermost rims are intermediate (typically An₅₀-An₈₀) with high FeO. Thus the Fe-enriched
168 phenocryst compositions overlap with the rims of sieved crystals. Microlite compositions
169 range from An₄₉ to An₈₃ and follow the same Fe-enrichment trend as the rims of sieved
170 crystals. Microlite cores tend to be more anorthitic and more Fe-rich than rims (figure 2).
171 Material from crystal clusters and mafic inclusions has composition An₅₂-An₈₉ and also
172 follows the Fe-enrichment trend, overlapping almost exactly with the microlites. Similar
173 patterns can be seen for MgO (figure 2).

174 175 **Amphibole**

176 Amphibole compositions (table 4) range from Mg-hornblende to pargasite (Leake et al. 1997).
177 The phenocrysts show limited correlation among cations. Al^T correlates positively (R² ~ 0.6,
178 figure 3a) with (Na+K)^A reflecting the edenite substitution, Si^T + [] = Al^T + (Na+K)^A. In
179 contrast, there is a poor correlation between Al^T and Al^{vi} or Mg^{vi} (figure 3b), or between Mn^{vi}
180 and Ti^{vi}, reflecting little control by the Tschermakite substitutions, Si^T + Mg^{vi} = Al^T + Al^{vi}
181 and Si^T + Mn^{vi} = Al^T + Ti^{vi}. Microphenocrysts, microlites, amphibole fragments and mafic
182 amphiboles cover a much wider range of compositions (figure 3). They extend the correlation
183 of Al^T with (Na+K)^A to higher Al^T, and also show a good correlation between Al^T and Al^{vi}, in
184 contrast to the phenocrysts. For phenocrysts, Al^T correlates negatively with Mg^{vi}. However,

185 the microlites, microphenocrysts, fragments and mafic amphiboles show a positive correlation
186 (figure 3b). Mg-number is also higher for the mafic amphiboles (Mg# 68-89) and microlites
187 and microphenocrysts (Mg# 63-84) than that of the phenocrysts (Mg# 61-70).
188

189 **Orthopyroxene**

190 Orthopyroxene phenocrysts (table 5) are fairly homogeneous, with Mg# 58-62 and 2-4 mol%
191 Wo. Some orthopyroxene phenocrysts have euhedral, zoned rims, which are significantly
192 more Mg-rich in composition (Mg# 63-74) than the cores. Mg-number shows a negative
193 correlation with Mn, although not with other minor elements (Ti, Al). Microphenocrysts
194 overlap in composition with the phenocrysts, with Mg# 59-63). However, microlites are
195 significantly richer in Al, Ca, Ti and Mg (Mg# 58-74), and poorer in Mn than the phenocrysts
196 (figure 4). The microlites overlap in composition with orthopyroxene from mafic inclusions
197 and crystal clusters (Mg# 59-74).
198

199 **Clinopyroxene**

200 Microphenocrysts, microlites, mafic clinopyroxenes and overgrowths on orthopyroxene
201 phenocrysts are all indistinguishable in composition, typically with Wo_{30-47} and En_{40-50} (figure
202 5). Mg decreases as Ca increases, while of the minor elements, Al correlates positively with
203 Ti and negatively with Mn.
204

205 **Fe-Ti oxides**

206 Magnetite occurs as microphenocrysts, microlites and in mafic inclusions and crystal clusters.
207 The compositions differ only in TiO_2 content (table 6; figure 6). Microlites and mafic
208 titanomagnetites are more Ti-rich than microphenocrysts. In general, microphenocryst rims
209 are slightly enriched in Ti compared with the cores. Minor elements (Al, Mg and Mn) show
210 no consistent variation. Rare crystals of pure magnetite are found.
211

212 **ESTIMATES OF TEMPERATURE AND OXYGEN FUGACITY**

214 **2-pyroxene temperatures**

215 Temperature estimates were made from coexisting orthopyroxene-clinopyroxene microlite or
216 microphenocryst pairs, using the method of Andersen et al. (1993). Temperatures estimated in
217 this way vary widely, from 903 °C to 1142 °C (n = 15), with an average of ~ 1070 °C.
218 Temperatures estimated from mafic inclusions and crystal clusters are higher, 1074 - 1196 °C
219 (n = 5), with an average of ~ 1110 °C. In particular, orthopyroxene phenocrysts are more Fe-
220 rich and Ca-poor than the microlites, zoned phenocryst rims and mafic orthopyroxene,
221 consistent with lower temperatures. QUILF (Andersen et al. 1993) used in single-pyroxene
222 mode (Murphy et al. 2000) gave typical orthopyroxene phenocryst core temperatures of 800-
223 900 °C (average ~ 850 °C, n=77). Phenocryst rims are typically slightly hotter (average ~870
224 °C, n=61), with clearly zoned phenocryst rims significantly hotter but variable (average
225 ~1000 °C, n=30). Microphenocryst core and rim temperatures compare closely to those of the
226 phenocrysts. These temperatures are consistent with those estimated for phenocrysts from
227 Phase I of the eruption (Murphy et al. 2000). Mafic inclusion orthopyroxenes consistently
228 gave higher orthopyroxene temperatures (average ~ 1070 °C, n=19). We note that
229 orthopyroxenes in sample MVO1521 are slightly richer in Ca and Al, and have lower Mn,
230 than those in other samples. This results in hotter calculated temperatures (~1000 °C for both
231 cores and rims). The reason for this discrepancy is not clear.
232

233 **Ilmenite-titanomagnetite geothermobarometry**

234 Ilmenite occurs relatively rarely. However, temperature estimates were obtained from seven
235 coexisting ilmenite-titanomagnetite pairs (Andersen et al. 1993). Oxide inclusions in
236 hornblende, and oxides from glass-bearing crystal clots gave low temperatures and relatively
237 oxidising conditions (791-809 °C, NNO + 1.3, n = 4). Zoned microphenocrysts and microlites
238 gave higher temperatures and were slightly less oxidising (958-1017 °C, NNO + 0.5, n = 3).

239

240 **Hornblende-plagioclase temperature**

241 Temperature estimates were also obtained using the hornblende-plagioclase geothermometer
242 of Holland & Blundy (1994). One phenocryst pair gave a temperature of 844 °C. Mafic
243 inclusions and crystal clusters gave significantly higher temperatures, 809-947 °C (n=10),
244 although some of these temperatures fall outside the range recommended for the thermometer.

245

246

247 **DISCUSSION**

248

249 **Origin of crystal clots**

250 The crystal clots are coarse-grained and contain pristine glass, rather than a microcrystalline
251 groundmass. They consistently give low temperatures (790-810 °C) and relatively oxidised
252 conditions (NNO + 1.2 to NNO + 1.4) relative to the host andesite (~ NNO + 0.5). Similar
253 clots have been observed at island arc volcanoes worldwide (e.g. Garcia & Jacobson 1979). It
254 has been suggested that the clots may represent clusters of phenocrysts, breakdown products
255 of hornblende, cooler wall-rock material, disrupted cumulates or micro-xenoliths (e.g. Garcia
256 & Jacobson 1979; Stewart 1975; Scarfe & Fuji 1987; Arculus 1976; Arculus & Wills 1980).
257 At Soufrière Hills, the low temperatures, oxidising conditions and lack of hornblende suggest
258 that the most likely origin is a highly crystalline part of the chamber, probably close to the
259 walls. This is also consistent with previous interpretations of the origin of low-temperature
260 orthopyroxenes and quartz (Murphy et al. 2000).

261

262 **Minor element partitioning in minerals**

263

264 *Fe and Mg partitioning in plagioclase*

265 Microlites, microphenocrysts and mafic plagioclase all follow a trend of Fe-enrichment, in
266 comparison with typical phenocryst compositions, which describe a shallow trend. The same
267 pattern, although with greater scatter, is also seen for Mg contents. Partitioning of Fe and Mg
268 in plagioclase varies as a function of temperature and anorthite content (Bindeman et al.
269 1998). D_{Fe} also varies with oxygen fugacity (e.g. Phinney 1992; Wilke & Behrens 1999).
270 However, the range of fO_2 measured at Soufrière Hills is only ~ 1 log unit (this study; Murphy
271 et al. 2000), which is insufficient to produce strong changes in D_{Fe} according to the
272 relationships described by Phinney (1992) and Wilke & Behrens (1999).

273

274 However, the predicted partitioning behaviour does not fit the data well if only temperature
275 and X_{An} effects are taken into account (figure 7). The predicted effects of temperature are
276 relatively small, with FeO_{pl} contents increasing by 0.1 wt% for an increase in temperature
277 from 850°C to 1050 °C. Predicted FeO_{pl} decreases smoothly by 0.45 wt% with an increase of
278 X_{An} from 0.4 to 0.75. However, the analytical data show a positive trend for phenocrysts
279 which cannot be produced even by the combined effects of T and X_{An} and suggests an effect
280 of melt composition as well as temperature. This is confirmed by using the partitioning data
281 of Bindeman et al. (1998) to calculate $FeO_{(pl)}$ and $MgO_{(pl)}$ for the experimental, H_2O -saturated
282 plagioclase-glass compositions of Couch et al. (2003a). The experimental glasses show a
283 small decrease in both $FeO_{(m)}$ and $MgO_{(m)}$ associated with crystallisation, over a temperature

284 range from 970 °C to 830 °C (Couch et al. 2003a). No plagioclase compositions are reported,
285 however X_{An} are given. We calculated $FeO_{(pl)}$ and $MgO_{(pl)}$ corresponding to experimental X_{An}
286 and T from Couch et al. (2003a), using Bindeman et al. (1998) partitioning data. The results
287 (black diamonds, figure 7) match the observed positive correlations for phenocrysts, although
288 $MgO_{(pl)}$ is a little low. This is consistent with the conclusions of Ruprecht & Wörner (2007)
289 for El Misti volcano, Peru. They identified major resorptions associated with increased
290 $FeO_{(pl)}$, which showed a steep, positive Fe- X_{An} correlation. They ascribed these to
291 compositional mixing through mafic recharge. In contrast, resorptions with no change in
292 $FeO_{(pl)}$ showed a flat Fe- X_{An} profile and were attributed to thermal effects (Ruprecht &
293 Wörner 2007), whether due to latent heat (Blundy et al. 2006) or a self-mixing scenario
294 involving convection in the resident magma (Couch et al. 2001).

295
296 Decompression crystallisation can occur rapidly (e.g. Couch et al. 2003b) so kinetic effects
297 should also be considered as a possible explanation for enrichment in Fe and Mg. If crystal
298 growth is more rapid than incompatible element diffusion in the melt, then a boundary layer
299 may form around the growing crystal, that is enriched in incompatible elements. For elements
300 moderately incompatible in plagioclase (such as Fe and Mg), these effects may result in
301 approximately 30-50% enrichment in the melt (Bottinga et al. 1966; Bacon 1989). Therefore,
302 it is plausible that some of the Fe-enrichment of microlites and mafic plagioclase at lower X_{An}
303 (e.g. An_{50} - An_{70}) may have been affected by kinetics. However, the positive correlation of Fe
304 with X_{An} still requires Fe variation in the melt; kinetic effects also cannot account for the very
305 high X_{An} contents (up to An_{90}) in microlites. Finally, microlite rims are less An-rich and have
306 lower Fe contents than the cores, which is inconsistent with crystallisation dominated by
307 kinetic factors.

308
309 The whole-rock FeO and MgO contents of basaltic andesite inclusions (Zellmer et al. 2003a)
310 are substantially higher (~9 wt%, ~4.2 wt%) than those of the andesite (~6.5 wt% FeO, ~3
311 wt% MgO). The temperatures calculated from 2-pyroxene geothermometry are also
312 considerably higher for the basaltic andesite (~1050 – 1100 °C) than the andesite (~850 °C).
313 The high-Fe, high-Mg, high- X_{An} analyses of sieved and mafic inclusion plagioclase are
314 therefore consistent with crystallisation from the hotter, more mafic environment in the
315 basaltic andesite. The microlite analyses are chemically indistinguishable from the mafic
316 plagioclase, thus it seems likely that they also crystallised in a hotter, more mafic
317 environment. The inflection in FeO at approximately An_{75} in the Montserrat data (not
318 observed for El Misti) suggests that the trend described by the sieved and mafic plagioclase
319 reflects fractional crystallisation, with $FeO_{(m)}$ initially increasing, before starting to decrease
320 with continued crystallisation. We suggest that this is probably related to early crystallisation
321 of pyroxenes in the mafic inclusions, followed by Fe-Ti oxides, which would result in falling
322 $FeO_{(m)}$. This implies that the basaltic andesite inclusions were largely liquid when they mixed
323 into the andesite.

324 325 *Mg, Ca, Ti and Al partitioning in pyroxene*

326 Orthopyroxene microlites, zoned phenocryst rims and mafic inclusion orthopyroxenes all
327 have higher contents of Al, Ti, Ca and Mg, as well as higher Mg#, than phenocryst and
328 microphenocryst orthopyroxene. For a given Mg#, the solubility of the Ca-component
329 increases with increasing temperature, while at constant Ca content, the Mg# increase with
330 temperature (Lindsley 1983). Ti and Al concentrations in orthopyroxene also increase with
331 temperature (Beattie 1993). These data therefore indicate that the mafic orthopyroxene,
332 microlites and zoned phenocryst rims all formed at hotter temperatures than the phenocrysts
333 and microphenocrysts.

334
335 For clinopyroxene, the solubility of the enstatite component increases with increasing
336 temperature, while the solubility of the diopside component decreases (Sepp & Kunzman
337 2001; Lindsley 1983). There are no clinopyroxene phenocrysts to compare with the microlites
338 and mafic clinopyroxene, but the spread of Ca-Mg compositional data (see figure 5) suggests
339 a range of crystallisation temperatures. This is consistent with the high temperatures
340 calculated from coexisting clinopyroxene and orthopyroxene microlites (903-1142 °C), mafic
341 pyroxenes (1074-1196 °C) and zoned orthopyroxene rims (870-1040 °C), compared with the
342 low phenocryst temperatures (800-900 °C). Clinopyroxenes also show a wide variation in Ti
343 and Al contents. This has previously been ascribed to variation in growth rate, with high Ti-
344 Al pyroxenes forming during rapid growth, for example at high cooling rates as might be
345 expected for the mafic inclusions (Feeley & Dungan 1996).

346 *Ti in titanomagnetite*

348 The oxide microlites and mafic inclusion crystals are very similar in composition to the
349 microphenocrysts, but with higher Ti content. Increased Ti in titanomagnetite can result from
350 increasing temperature or decreasing oxygen fugacity (Frost & Lindsley 1991; Devine et al.
351 2003). The change in composition therefore suggests that the microlites crystallised at higher
352 temperatures than the microphenocrysts in the andesite.

353 **Interpretation of microlite and phenocryst compositions**

355 Taken together, the chemical data indicate that the microlites of plagioclase, orthopyroxene
356 and clinopyroxene crystallised in a hotter and more mafic environment than the phenocrysts
357 of the andesite, one similar to the mafic inclusions. The temperature of the mafic magma was
358 initially approximately 1050-1150 °C, on the basis of pyroxene compositions. Previously,
359 anomalously hot 2-pyroxene microlite temperatures were assumed to result from
360 disequilibrium growth (e.g. Murphy et al. 2000). We suggest instead that the microlites
361 probably originated in the mafic inclusions, and were transferred into the andesite following
362 initial mingling. Transfer of calcic plagioclase microlites is also envisaged for Mont Pelée,
363 Martinique (Martel et al. 2006). Continued decompression of the hybrid andesite causes
364 continued crystallisation on the mafic microlite cores, producing zoned microlites and
365 microphenocrysts (e.g. Couch et al. 2003a, Murphy et al. 2000).

367 Reversely zoned and cpx-rimmed orthopyroxene phenocrysts both indicate heating.
368 Clinopyroxene from the reaction rims is compositionally indistinguishable from mafic
369 inclusion clinopyroxene, so we infer that these reaction rims form when orthopyroxene
370 phenocrysts are incorporated into the basaltic andesite. In contrast, the reversely zoned
371 orthopyroxenes experienced conductive heating in the andesite. Multiple rim zones imply
372 more than one episode of heating, suggesting multiple injections of mafic material. This is
373 consistent with the occurrence of seismic crises at Montserrat in 1896-1897, 1933-1937 and
374 1966-1967, which were interpreted as periods of magma intrusion (MacGregor 1938; Perret
375 1939; Shepherd et al. 1971). These textures are analogous to the thermal breakdown rims seen
376 in hornblende (see earlier).

377
378 The amphibole data show a good positive correlation of Al^T and $(Na+K)^A$, suggesting a strong
379 role of the temperature-sensitive edenite substitution. Mafic amphiboles and small grains have
380 higher Al^T while phenocrysts have low Al^T . This is consistent with the mafic material
381 crystallising at higher temperatures (e.g. Bachmann & Dungan 2002). In contrast, there is
382 only a weak trend of decreasing Mg^{vi} with increasing Al^T , indicating much weaker role for the
383 pressure-dependent Tschermakite substitution. However, mafic amphiboles and small grains

384 are enriched in both Mg and Al (see figure 3). This is consistent with lower silica activity in
385 the melt due to the presence of more mafic magma (Sato et al. 2005). We therefore suggest
386 that the small grains predominantly represent material that originated in the mafic inclusions
387 and was transferred to the magma. This explains the occurrence of hornblende in the
388 groundmass; experiments have consistently shown that hornblende is not stable in the
389 andesite at low pressures (e.g. Barclay et al. 1998; Rutherford & Devine 2003).

390

391 The high TiO₂ contents of the microlites are also consistent with hotter crystallisation
392 conditions. Some titanomagnetite microphenocryst rims are zoned, with slightly more Ti-rich
393 compositions than their cores. This has previously been ascribed to heating of the andesite
394 (Devine et al. 1998; Devine et al. 2003), which could be related to the release of latent heat
395 during decompression crystallisation (Blundy et al. 2006) or to mafic recharge (Devine et al.
396 2003). However, heating due to crystallisation should affect all titanomagnetite crystals
397 equally, whereas varying degrees of Ti-enrichment are observed. These zoned crystals
398 therefore probably experienced transient heating in the vicinity of the influxing basaltic
399 andesite, analogous to the zoned orthopyroxene phenocrysts.

400

401 **Interpretation of zoned plagioclase phenocryst compositions**

402 Previously, oscillatory zoning in plagioclase has been attributed to various processes,
403 including mixing with mafic or silicic magma (e.g. Singer et al. 1995; Ginibre et al. 2002),
404 thermal perturbations (e.g. Couch et al. 2001); kinetics (Bottinga et al. 1966; Allegre et al.
405 1981), or decompression (Nelson & Montana 1992). However, this study shows that the
406 enrichment of Fe and Mg in plagioclase at intermediate anorthite content seems to be a robust
407 method for identifying plagioclase that crystallised in a more mafic environment. We
408 therefore apply this to traverses of plagioclase phenocrysts in the andesite. Figure 8 shows Fe-
409 X_{An} compositions for traverses across oscillatory zoned phenocrysts. The data show that very
410 few points in the oscillatory zoned crystals are related to influx of mafic magma. Conversely,
411 most of the points analysed describe a flat Fe-X_{An} profile. The few Fe-enriched points are
412 mostly found in the outermost crystal rim, or where a narrow sieved zone is present in the
413 traverse. Traverses through the clear rims of strongly sieved crystals show that the mafic
414 crystallisation trend starts at ~ An₈₅ and passes through the inflection point at ~0.6 wt% FeO
415 (figure 8), as previously described. The lack of Fe-enriched compositions in oscillatory zoned
416 crystals suggests that most of the oscillatory zonation is produced by other processes, and that
417 most of the resorption horizons observed relate to perturbations of temperature and/or p_{H₂O}
418 in the storage chamber. Some plagioclase from Montserrat have constant Sr contents despite
419 strong variations in X_{An} (Zellmer et al. 2003b); these are also consistent with this
420 interpretation. The occurrence of Fe-rich outer rims suggests that contact with mafic magma
421 was one of the last things to happen prior to eruption of these crystals.

422

423 **Transfer of crystals between mafic inclusions and andesite**

424 The nature of interaction between mafic and silicic magmas depends strongly on the relative
425 proportion of the incoming mafic magma, as well as the contrast of temperature and viscosity
426 between the two end-members (Sparks & Marshall 1986). In the Soufrière Hills magma, the
427 macroscopic mafic inclusions are typically rounded to ellipsoidal, with well-defined, smooth
428 or crenulated margins that may be chilled (Murphy et al. 2000; J. Barclay, personal
429 communication), indicating strong undercooling of the mafic magma against the host
430 andesite. Given these observations and the strong temperature contrast between the end-
431 members (~1100 °C for the basaltic andesite, *c.f.* ~ 840 °C for the andesite; Barclay et al.
432 1998), it is unlikely that efficient stirring and hybridisation took place while the two magmas
433 were liquid (Sparks & Marshall 1986). The presence in the mafic inclusions of sieved

434 plagioclase, orthopyroxene overgrown by clinopyroxene, and strongly reacted hornblende,
435 originally derived from the andesite, shows that some mixing did take place, in the form of
436 transfer of phenocrysts from the andesite to the mafic magma. However, the sieved
437 plagioclase crystals have clear, calcic overgrowths with an inflection in Fe-X_{An} , indicating
438 crystallisation in the mafic magma, so incorporation of the crystals must have occurred soon
439 after injection of the basaltic andesite, while it was still largely liquid. The void-filling shape
440 of the vesicles in the mafic inclusions and crystal clusters (see figure 1) suggests that the
441 cooling magma formed a strong crystal framework and that vesiculation occurred during
442 cooling. The strong framework of crystals would make the inclusions susceptible to later
443 mechanical disaggregation (Martin et al. 2006), and we suggest that this is the most likely
444 mechanism for transferring the mafic microlites to the andesite. This is supported by the wide
445 size distribution of mafic material, from macroscopic inclusions down to crystal clusters and
446 isolated crystals, including the strongly reacted plagioclase, orthopyroxene and hornblende
447 crystals which had started out in the andesite. Mechanical disaggregation of inclusions was
448 also envisaged at Tatara – San Pedro volcano, Chile (Feeley & Dungan 1996).
449

450 However, the timing and mechanism of disaggregation is unclear. Possible mechanisms
451 include mechanical abrasion of the chilled margins (Feeley & Dungan 1996), wholesale
452 breaking of the inclusions (Martin et al. 2006), or plastic deformation (Blake & Fink 2000).
453 Disaggregation could take place in the magma chamber, during ascent in the conduit, or
454 during emplacement of the dome rocks. The viscosity of the host andesite is estimated to be \sim
455 7×10^6 Pa s in the magma chamber, rising to approximately 10^{13} - 10^{14} Pa s at the surface due
456 to degassing and decompression crystallisation (Sparks et al. 2000). The ellipsoidal shape of
457 some of the larger inclusions (Murphy et al. 2000) indicates that some plastic deformation
458 took place during quenching. However, plastic deformation will effectively cease once a
459 significant chilled margin is formed (Blake & Fink 2000). This will likely happen quickly,
460 given the large temperature contrast between the two magmas, and this is indicated by
461 theoretical constraints (Plechov et al. 2008b) which show that thermal equilibration of
462 enclaves with resident magma occurs within hours to days. Therefore most of the
463 disaggregation must have occurred after this initial stage of magma mingling.
464

465 Once the inclusions are strongly crystalline, they will undergo brittle deformation (Sparks et
466 al. 2000) and may not transfer much heat to the host andesite in doing so. Brittle deformation
467 was inferred at Nea Kameni, Santorini, from small fractures and bent crystals in mafic
468 inclusions, the most angular of the inclusions commonly being found in the centre of
469 inclusion clusters (Martin et al. 2006). The degree of deformation is related to the shear stress
470 experienced by the enclave (Blake & Fink 2000), and will therefore increase with host magma
471 viscosity, and with eruption rate. Since the viscosity of the andesite increases by several
472 orders of magnitude during ascent, due largely to decompression crystallisation (Sparks et al.
473 2000), it seems likely that the majority of deformation and break-up of the inclusions
474 occurred during ascent in the conduit. The presence of mafic-derived microlites in pumiceous
475 material (MVO1523 and MVO1524) precludes transfer of material during dome
476 emplacement.
477

478 The rapid re-equilibration times of titanomagnetite (Hammond & Taylor 1982; Venezky &
479 Rutherford 1999) can provide clues to the timing of inclusion disaggregation. The oxide
480 microlites are more Mg-rich than microphenocrysts from the andesite. The grain size of the
481 microlites analysed is typically 20 μm ; grains of this size should re-equilibrate in
482 approximately 50 days at 825 °C, 30 days at 850 °C, or only 11 days at 900 °C (Venezky &
483 Rutherford 1999). The pre-eruptive temperature of the andesite was \sim 850 °C, possibly rising

484 to ~900 °C during ascent due to the release of latent heat of crystallisation (Couch et al.
485 2003a; Blundy et al. 2006). This suggests that the time between disaggregation and eruption
486 was in the range 10-30 days, and therefore that disaggregation probably occurred during
487 ascent. This suggests ascent rates, from ~6 km to the surface, of 8-25 m/h. These rates are
488 very similar to estimates of ascent rate for Mount Unzen, Japan (Venezky & Rutherford 1999)
489 as well as for Soufrière Hills using different methods (e.g. Rutherford & Devine 2003).

490

491 **Implications**

492 The presence of mafic microlites in the groundmass of the Soufrière Hills andesite means that
493 the proportion of mafic material in the system is greater than previously thought. It provides
494 an explanation for the presence of ubiquitous clinopyroxene in some phase equilibrium
495 studies (Couch et al. 2003a), where none is observed in the andesite. In terms of the “reactive
496 magma” concept put forward by Pichavant et al. (2007), the bulk groundmass cannot be
497 regarded as a good starting material for phase equilibrium experiments, because a significant
498 fraction of the microlites are not part of the reactive magma, but are incorporated from an
499 external source, the mafic inclusions.

500

501 **CONCLUSIONS**

502 The groundmass of the andesite magma at Soufrière Hills volcano, Montserrat contains
503 microlites that originated in quenched mafic inclusions. Many of the microlites have different
504 compositions from the andesite phenocrysts, but are chemically indistinguishable from the
505 compositions of crystals found in basaltic andesite inclusions. The basaltic andesite initially
506 had a temperature of ~1050-1100 °C and quenched rapidly to form mafic inclusions. Some
507 phenocrysts from the andesite were incorporated into the inclusions during this time, resulting
508 in the formation of sieved plagioclase textures, clinopyroxene overgrowths on orthopyroxene
509 and quartz, and breakdown of hornblende. Following cooling and vesiculation of the mafic
510 magma, mass transfer occurred by brittle disaggregation of the inclusions. Plagioclase,
511 orthopyroxene, clinopyroxene and titanomagnetite microlites were transferred from the
512 inclusions to the andesite. Disaggregation would have required high shear stress and probably
513 occurred during flow in the conduit. The discovery of mafic microlites in the andesite means
514 that groundmass material is an inappropriate starting composition for experimental phase
515 petrology. Care should also be taken when using groundmass textures to calculate crystal size
516 distributions, or infer growth or ascent rates.

517

518

519 **ACKNOWLEDGEMENTS**

520 This study is published with the permission of the Director of the Montserrat Volcano
521 Observatory. MCSH was supported by a Junior Research Fellowship at Trinity College,
522 University of Cambridge. We are grateful to Chris Hayward for his assistance with electron
523 microprobe analysis. The manuscript was improved following constructive reviews from
524 Georg Zellmer and an anonymous reviewer.

525

526

527 **REFERENCES**

528 Allègre CJ, Provost, A & Jaupart C (1981) Oscillatory zoning: A pathological case of crystal
529 growth. *Nature* 294: 223-228
530 Anderson AT (1976) Magma mixing: Petrological process and volcanological tool. *J*
531 *Volcanol Geotherm Res* 1: 3-33

532 Andersen DJ, Lindsley DH & Davidson PM (1993) QUILF: A Pascal program to assess
 533 equilibria among Fe-Mg-Ti oxides, pyroxenes, olivine and quartz. *Comp Geosci* 19: 1333-
 534 1350
 535 Arculus RJ (1976) Geology and geochemistry of the alkali basalt-andesite association of
 536 Grenada, Lesser Antilles island arc. *Geol Soc Am Bull* 87: 612-624
 537 Arculus RJ & Wills, KJA (1980) The petrology of plutonic blocks and inclusions from the
 538 Lesser Antilles island arc. *J Petrol* 21: 743-799
 539 Bachmann O & Dungan MA (2002) Temperature-induced Al-zoning in hornblendes of the
 540 Fish Canyon magma, Colorado. *Am Mineral* 87: 1062-1076
 541 Bacon CR (1986) Magmatic inclusions in silicic and intermediate volcanic rocks. *J Geophys*
 542 *Res* 91: 6091-6112
 543 Bacon CR (1989) Crystallization of accessory phases in magmas by local saturation adjacent
 544 to phenocrysts. *Geochim Cosmochim Acta* 53, 1055-1066
 545 Barclay J, Rutherford MJ, Carroll MR, et al (1998) Experimental phase equilibria constraints
 546 on pre-eruptive storage conditions of the Soufrière Hills magma. *Geophys Res Lett* 25: 3437-
 547 3440
 548 Beattie P (1993) Olivine-melt and orthopyroxene-melt equilibria. *Contrib Mineral Petrol* 115:
 549 103-111
 550 Bindeman IN, Davis AM & Drake MJ (1998) Ion microprobe study of plagioclase-basalt
 551 partition experiments at natural concentration levels of trace elements. *Geochim Cosmochim*
 552 *Acta* 62: 1175-1193
 553 Blake S & Fink JH (2000) On the deformation and freezing of enclaves during magma
 554 mixing. *J Volcanol Geotherm Res* 95: 1-8
 555 Blundy J, Cashman K & Humphreys M (2006) Magma heating by decompression-driven
 556 crystallization beneath andesite volcanoes. *Nature* 443: 76-80
 557 Blundy JD & Sparks RSJ (1992) Petrogenesis of mafic inclusions in granitoids of the
 558 Adamello Massif, Italy. *J Petrol* 33: 1039-1104
 559 Bottinga Y, Kudo A & Weill D (1966) Some observations on oscillatory zoning and
 560 crystallization of magmatic plagioclase. *Am Mineral* 51: 792-806
 561 Browne BL, Eichelberger JC, Patina LC et al (2006) Generation of porphyritic and
 562 equigranular mafic enclaves during magma recharge events at Unzen Volcano, Japan. *J Petrol*
 563 47: 301-328
 564 Buckley VJE, Sparks RSJ & Wood BJ (2006) Hornblende dehydration reactions during
 565 magma ascent at Soufrière Hills Volcano, Montserrat. *Contrib Mineral Petrol* 151: 121-140
 566 Cashman KV (1992) Groundmass crystallization of Mount St. Helens dacite, 1980-1986: A
 567 tool for interpreting shallow magmatic processes. *Contrib Mineral Petrol* 109: 431-449
 568 Clynne MA (1999) A complex magma mixing origin for rocks erupted in 1915, Lassen Peak,
 569 California. *J Petrol* 40: 105-132.
 570 Couch S, Sparks RSJ & Carroll MR (2001) Mineral disequilibrium in lavas explained by
 571 convective self-mixing in open magma chambers. *Nature* 411: 1037-1039
 572 Couch S, Harford CL, Sparks RSJ & Carroll MR (2003a) Experimental constraints on the
 573 conditions of formation of highly calcic plagioclase microlites at the Soufrière Hills Volcano,
 574 Montserrat. *J Petrol* 44: 1455-1475
 575 Couch S, Sparks RSJ & Carroll MR (2003b) The kinetics of degassing-induced crystallization
 576 at Soufrière Hills Volcano, Montserrat. *J Petrol* 44: 1477-1502
 577 Devine JD, Murphy MD, Rutherford MJ et al (1998) Petrologic evidence for pre-eruptive
 578 pressure-temperature conditions and recent reheating, of andesitic magma erupting at the
 579 Soufrière Hills Volcano, Montserrat, W.I. *Geophys Res Lett* 25: 3669-3672

580 Devine JD, Rutherford MJ, Norton GE et al (2003) Magma storage region processes inferred
581 from geochemistry of Fe-Ti oxides in andesitic magma, Soufriere Hills Volcano, Montserrat,
582 W.I. *J Petrol* 44: 1375-1400

583 Eichelberger JC (1978) Andesitic volcanism and crustal evolution. *Nature* 275: 21-27

584 Eichelberger JC (1980) Vesiculation of mafic magma during replenishment of silicic magma
585 chambers. *Nature* 288: 446-450

586 Feeley TC & Dungan MA (1996) Compositional and dynamic controls on mafic-silicic
587 magma interactions at continental arc volcanoes: Evidence from Cordón El Guadal, Tatara -
588 San Pedro Complex, Chile. *J Petrol* 37: 1547-1577

589 Frost BR & Lindsley DH (1991) Occurrence of iron-titanium oxides in igneous rocks. *Rev in*
590 *Mineral* 25: 433-468

591 Garcia MO & Jacobson SS (1979) Crystal clots, amphibole fractionation and the evolution of
592 calc-alkaline magmas. *Contrib Mineral Petrol* 69: 319-327

593 Ginibre C, Wörner G & Kronz A (2002) Minor- and trace-element zoning in plagioclase:
594 implications for magma chamber processes at Parinacota volcano, northern Chile. *Contrib*
595 *Mineral Petrol* 143: 300-315

596 Hammond PA & Taylor LA (1982) The ilmenite/ titanomagnetite assemblage: kinetics of re-
597 equilibration. *Earth Planet Sci Lett* 61: 143-150.

598 Holland T & Blundy J (1994) Non-ideal interactions in calcic amphiboles and their bearing
599 on amphibole-plagioclase thermometry. *Contrib Mineral Petrol* 116: 433-447

600 Leake BE, Wooley AR, Arps CES (1997) Nomenclature of amphiboles: Report of the
601 subcommittee on amphiboles of the International Mineralogical Association, Commission on
602 new minerals and mineral names. *Can Mineral* 35: 219-246

603 Lindsley DH (1983) Pyroxene thermometry. *Am Mineral* 68: 477-493

604 MacGregor AG (1938). The Royal Society expedition to Montserrat, B.W.I. The volcanic
605 history and petrology of Montserrat, with observations on Mt Pele, in Martinique. *Phil Trans*
606 *Roy Soc London* 229, 1-90

607 Martel C, Radadi Ali A, Poussineau S et al (2006) Basalt-inherited microlites in silicic
608 magmas: evidence from Mount Pelée (Martinique, French West Indies). *Geology* 34: 905-908

609 Martin VM, Pyle DM & Holness MB (2006) The role of crystal frameworks in the
610 preservation of enclaves during magma mixing. *Earth Planet Sci Lett* 248: 787-799

611 Melnik O & Sparks RSJ (1999) Nonlinear dynamics of lava dome extrusion. *Nature* 402: 37-
612 41

613 Murphy MD, Sparks RSJ, Barclay J et al (2000) Remobilization of andesite magma by
614 intrusion of mafic magma at the Soufrière Hills Volcano, Montserrat, West Indies. *J Petrol*
615 41: 21-42

616 Nelson ST & Montana A (1992) Sieve-textured plagioclase in volcanic rocks produced by
617 rapid decompression. *Am Mineral* 77: 1242-1249

618 Perret F (1939). The volcano-seismic crisis at Montserrat 1933-1937. *Publ Carnegie Inst*
619 *Washington* 512, 76 pp.

620 Phinney WC (1992) Partition coefficients for iron between plagioclase and basalt as a
621 function of oxygen fugacity: Implications for Archaean and lunar anorthosites. *Geochim*
622 *Cosmochim Acta* 56: 1885-1895

623 Pichavant M, Costa F, Burgisser A et al (2007) Equilibration scales in silicic to intermediate
624 magmas – Implications for experimental studies. *J Petrol* 48: 1955-1972

625 Plechov PYu, Tsai AE, Shcherbakov VD et al (2008a) Opacitization conditions of hornblende
626 in Bezymyanni Volcano andesites (March 30, 1956 eruption). *Petrol* 16, 19-35

627 Plechov PYu, Fomin IS, Melnik OE et al (2008b) Evolution of melt composition during
628 intrusion of basalts into a silicic magma chamber. *Moscow Univ Geol Bull* 63, 247-257

629 Ruprecht P & Wörner G (2007) Variable regimes in magma systems documented in
630 plagioclase zoning patterns: El Misti stratovolcano and Andahua monogenetic cones. *J*
631 *Volcanol Geotherm Res* 165: 142-162

632 Rutherford MJ & Hill PM (1993) Magma ascent rates from amphibole breakdown: An
633 experimental study applied to the 1980-1986 Mount St Helens eruptions. *J Geophys Res* 98,
634 19,667-19,685

635 Rutherford MJ & Devine JD (2003) Magmatic conditions and magma ascent as indicated by
636 hornblende phase equilibria and reactions in the 1995-2002 Soufrière Hills magma. *J Petrol*
637 44: 1433-1454

638 Sato H, Holtz F, Behrens H, Botcharnikov R & Nakada S (2005) Experimental petrology of
639 the 1991-1995 Unzen dacite, Japan. Part II: Cl/OH partitioning between hornblende and melt
640 and its implications for the origin of oscillatory zoning of hornblende phenocrysts. *J Petrol*
641 46: 339-354

642 Scarfe CM & Fuji T (1987) Petrology of crystal clots in the pumice of Mount St. Helens'
643 March 19, 1982 eruption: Significant role of Fe-Ti oxide crystallisation. *J Volcanol Geotherm*
644 *Res* 34: 1-14

645 Schumacher JC (1997) The estimation of the proportion of ferric iron in the electron-
646 microprobe analysis of amphiboles. *Can Mineral* 35: 238-246

647 Sepp B & Kunzman T (2001) The stability of clinopyroxene in the system CaO-MgO-SiO₂-
648 TiO₂ (CMST). *Am Mineral* 86: 265-270

649 Shepherd JB, Tomblin JF & Woo DA (1971). Volcano-seismic crisis in Montserrat, West
650 Indies, 1966-1967. *Bull Volcanol* 35, 143-163

651 Singer BS, Dungan MA & Layne GD (1995) Textures and Sr, Ba, Mg, Fe, K, and Ti
652 compositional profiles in volcanic plagioclase: Clues to the dynamics of calc-alkaline magma
653 chambers. *Am Mineral* 80 776-798

654 Sparks RSJ & Marshall LA (1986) Thermal and mechanical constraints on mixing between
655 mafic and silicic magmas. *J Volcanol Geotherm Res* 29: 99-124

656 Sparks RSJ, Murphy MD, Lejeune AM et al (2000) Control on the emplacement of the
657 andesite lava dome of the Soufrière Hills volcano, Montserrat by degassing-induced
658 crystallization. *Terra Nova* 12: 14-20

659 Stewart DC (1975) Crystal clots in calc-alkaline andesites as breakdown products of high-Al
660 amphiboles. *Contrib Mineral Petrol* 53: 195-204

661 Stormer JC (1983) The effects of recalculation on estimates of temperature and oxygen
662 fugacity from analyses of multi-component iron-titanium oxides. *Am Mineral* 66, 586-594.

663 Venezky DY & Rutherford MJ (1999) Petrology and Fe-Ti oxide re-equilibration of the 1991
664 Mount Unzen mixed magma. *J Volcanol Geotherm Res* 89 213-230

665 Wilke M & Behrens H (1999) The dependence of the partitioning of iron and europium
666 between plagioclase and hydrous tonalitic melt on oxygen fugacity. *Contrib Mineral Petrol*
667 137: 102-114

668 Zellmer GF, Hawkesworth CJ, Sparks RSJ et al (2003a) Geochemical evolution of the
669 Soufrière Hills Volcano, Montserrat, Lesser Antilles volcanic arc. *J Petrol* 44: 1349-1374

670 Zellmer GF, Sparks RSJ, Hawkesworth CJ et al (2003b) Magma emplacement and
671 remobilization timescales beneath Montserrat: Insights from Sr and Ba zonation in
672 plagioclase phenocrysts. *J Petrol* 44, 1413-1431

673
674

675 Figure 1. Back-scattered SEM images and photomicrographs of mineral textures in the
676 Soufrière Hills magma. a) Hornblende phenocryst with narrow, fine-grained decompression
677 breakdown rim (arrow). The interior of the crystal is partially replaced by black opacite. Field
678 of view 2.3 mm. b) Hornblende phenocryst with thick thermal breakdown rim, characterised

679 by coarse, clinopyroxene-rich reaction products, and alignment of individual grains with the
680 c-axis of the hornblende. Field of view 2.3 mm. c) Margin of orthopyroxene phenocryst with
681 reversely zoned rim. This crystal has a rim with two distinct reversely zoned sections (black
682 arrows). d) Vesicular mafic inclusion containing pyroxene (px), plagioclase (pl) and oxides
683 (ox). e) Crystal cluster comprising vesicular (ves) mafic material, plagioclase, clinopyroxene,
684 and yellow pargasitic hornblende (hb). Field of view ~1.1 mm. f) Crystal clot with equant
685 grains of orthopyroxene, plagioclase and oxides as well as vesicular glass. Crystal clots are
686 texturally distinct from mafic inclusions and crystal clusters, and probably represent cognate
687 material. g) Sieved plagioclase showing core, 'inner rim' and 'outer rim' referred to in text. h)
688 Typical andesite groundmass texture, comprising crystals of plagioclase (mid-grey), pyroxene
689 (light grey), and oxide (white) with vesicles (black) in greyish glass.

690
691 Figure 2. FeO and MgO contents of plagioclase, sorted by textural characteristics. Sieved
692 plagioclase (c and d) are significantly enriched in Fe and Mg compared with unaltered cores
693 and other phenocrysts (a and b). Plagioclase microlites and plagioclase in mafic inclusions (a
694 and b) are also strongly enriched in Fe and Mg, and are chemically indistinguishable from one
695 another, and from the sieved plagioclase.

696
697 Figure 3. Hornblende compositions in the Soufrière Hills magma. a) Al^T correlates well with
698 $(Na+K)^A$. Mafic hornblende is easily distinguished from phenocrysts in the andesite. Small
699 grains and microlites of hornblende overlap in composition with the mafic material. b) For
700 phenocrysts, Mg^{vi} correlates negatively with Al^T while for mafic hornblende and microlites,
701 there is a weak positive correlation.

702
703 Figure 4. Orthopyroxene compositions in the Soufrière Hills magma. Phenocrysts are
704 relatively homogeneous in composition. Distinctly zoned rims on phenocrysts have higher
705 Mg, Ca and Al, and lower Mn. Microlites and mafic inclusions have more Mg, Ca, Al rich
706 compositions compared with the phenocrysts.

707
708 Figure 5. Clinopyroxene compositions in the Soufrière Hills magma. Microphenocrysts,
709 microlites, mafic inclusion clinopyroxene and overgrowth rims on orthopyroxene phenocrysts
710 are all indistinguishable in composition, and cover a wide range of Mg, Al and Ti
711 compositions.

712
713 Figure 6. Titanomagnetite compositions. Microlites and mafic inclusion titanomagnetite are
714 significantly enriched in Ti compared with microphenocrysts.

715
716 Figure 7. Fe and Mg partitioning in plagioclase. Grey circles are plagioclase compositional
717 data (all textural types). Curves indicate FeO and MgO contents of plagioclase, calculated
718 from experimental partitioning data (Bindeman et al.1998), at constant temperature (labelled)
719 and constant melt composition, with varying X_{An} . Solid curves: 1.7 wt% FeO or 0.4 wt%
720 MgO in the melt. Dashed curve: 2.5 wt% FeO or 0.8 wt% MgO in the melt. Black diamonds
721 are experimental X_{An} from Couch et al.(2003a) with FeO_{pl} and MgO_{pl} calculated using their
722 experimental T and $FeO_{(m)}$ or $MgO_{(m)}$ and partitioning data from Bindeman et al.(1998). This
723 takes into account small changes in melt composition during crystallisation (see text for
724 details).

725
726 Figure 8. X_{An} vs wt% FeO for selected plagioclase phenocryst zoning traverses. Location of
727 each traverse is shown by the arrow or bar in the accompanying BSE images
728 (MVO1350_34p4 and MVO1350_31) or photomicrographs. Scale bar represents 100 μm .

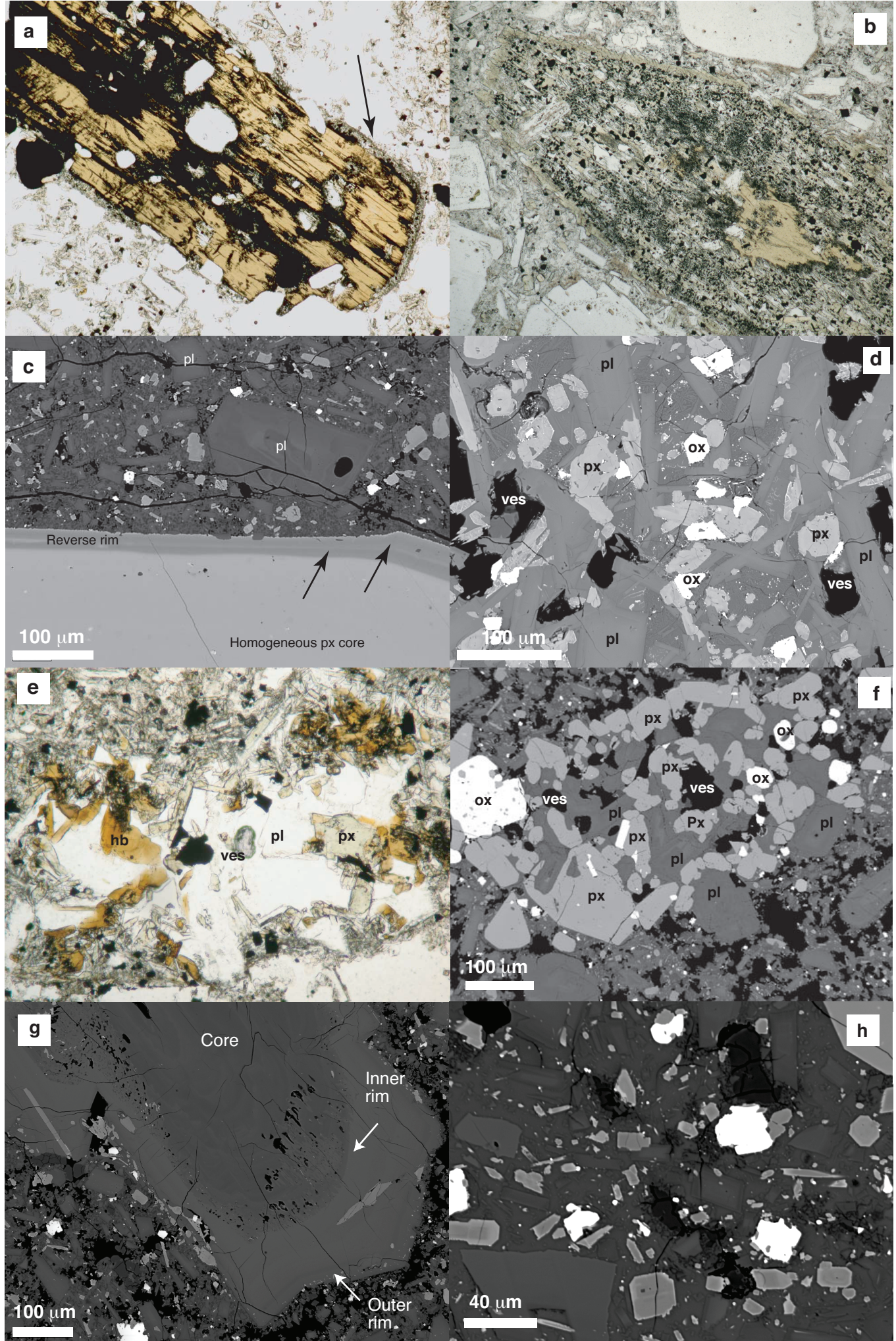


Figure 1

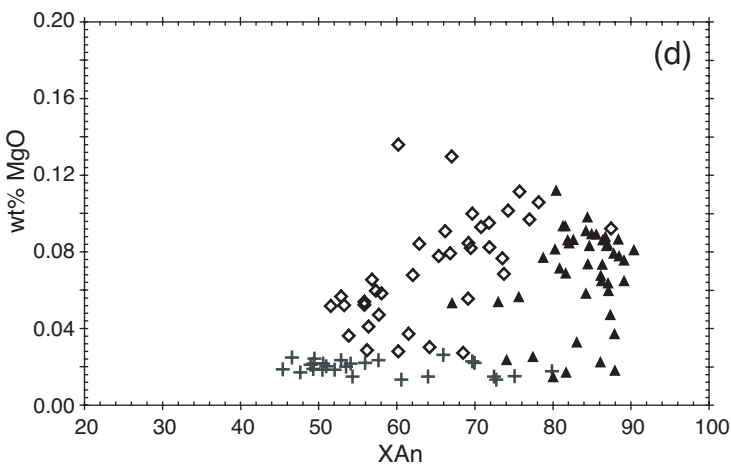
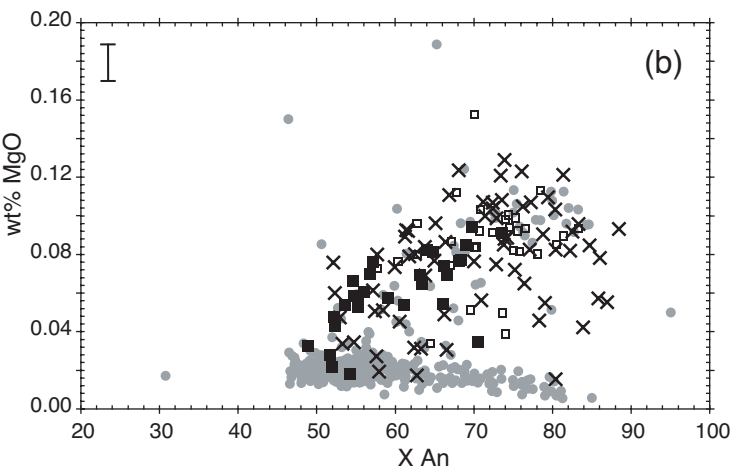
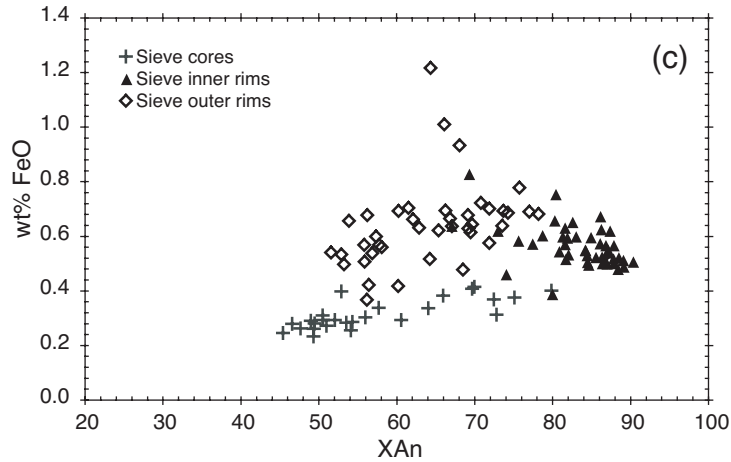
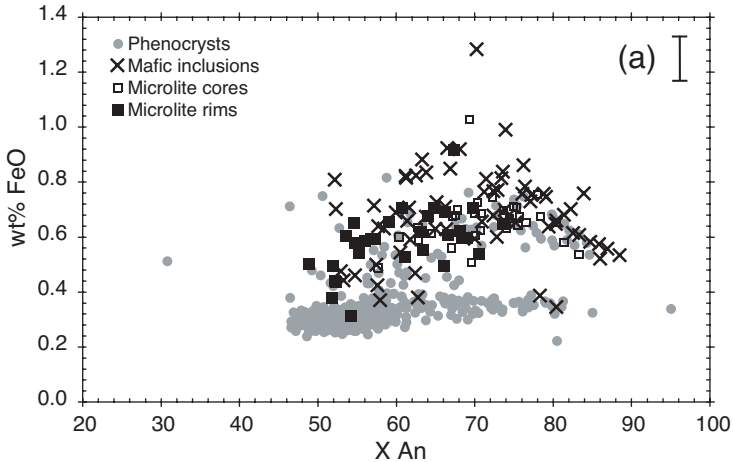


Figure 2

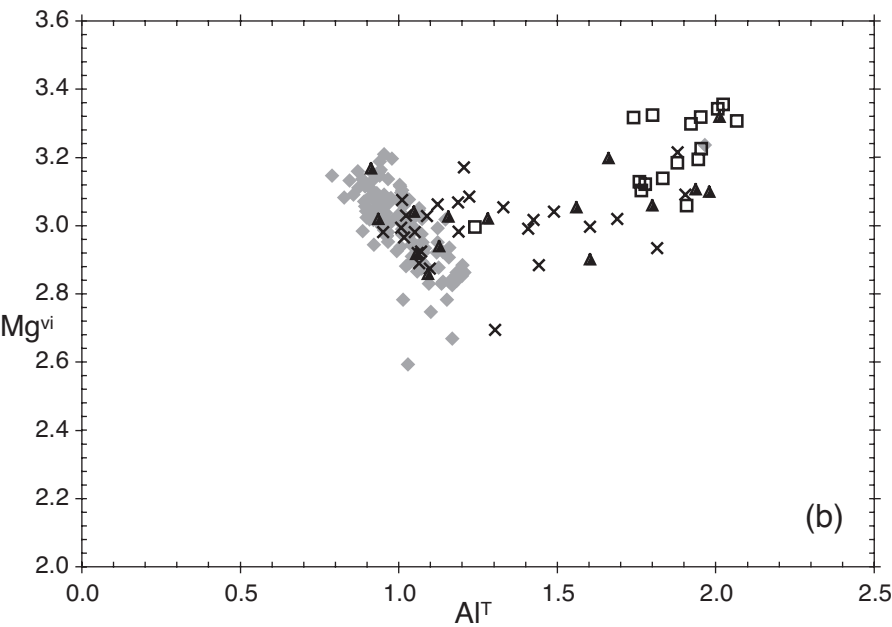
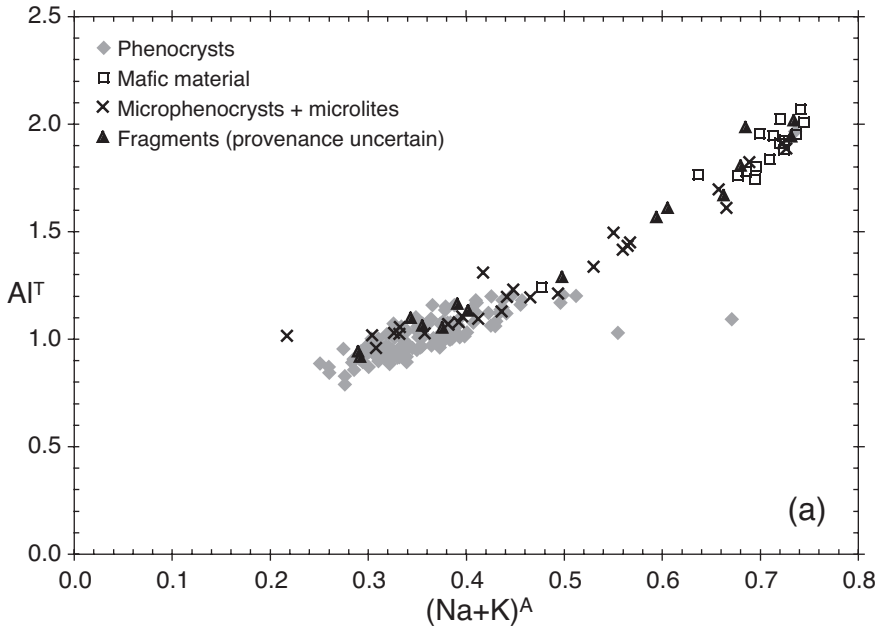
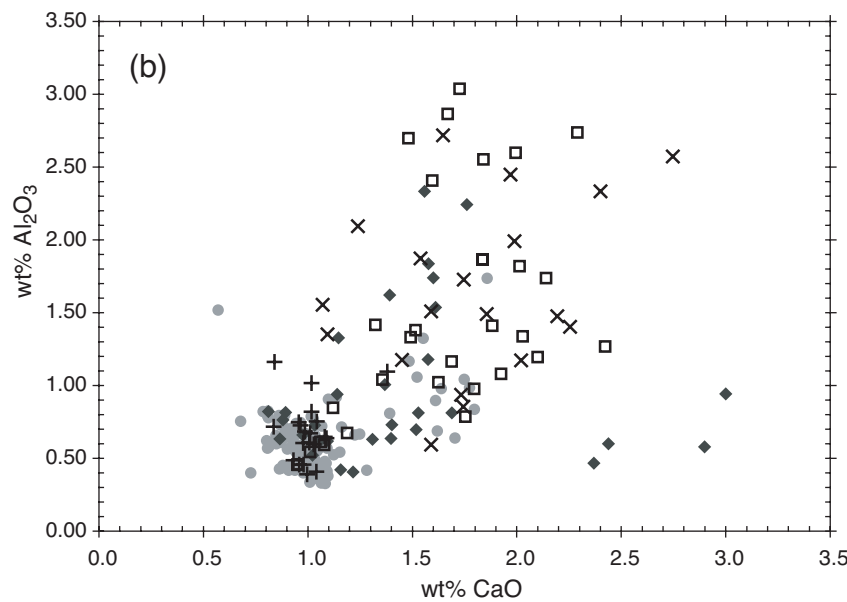
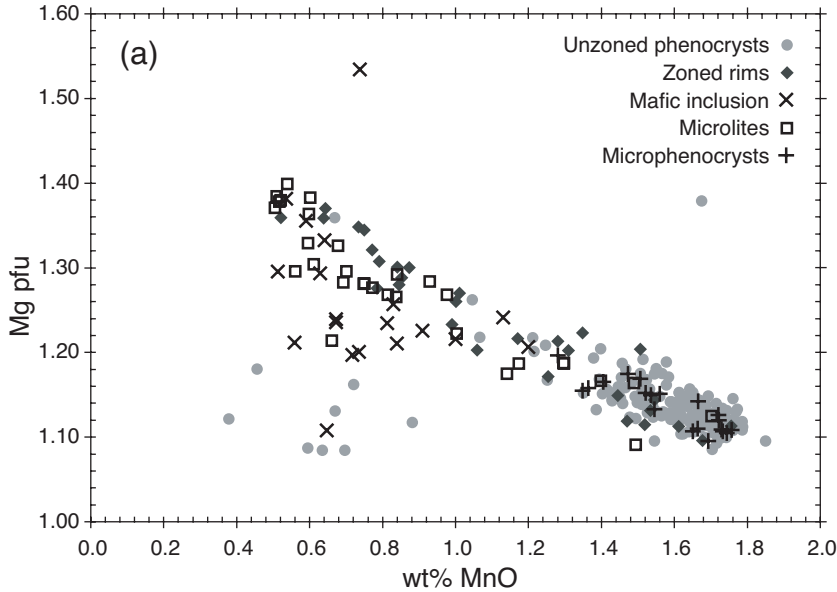


Figure 3.



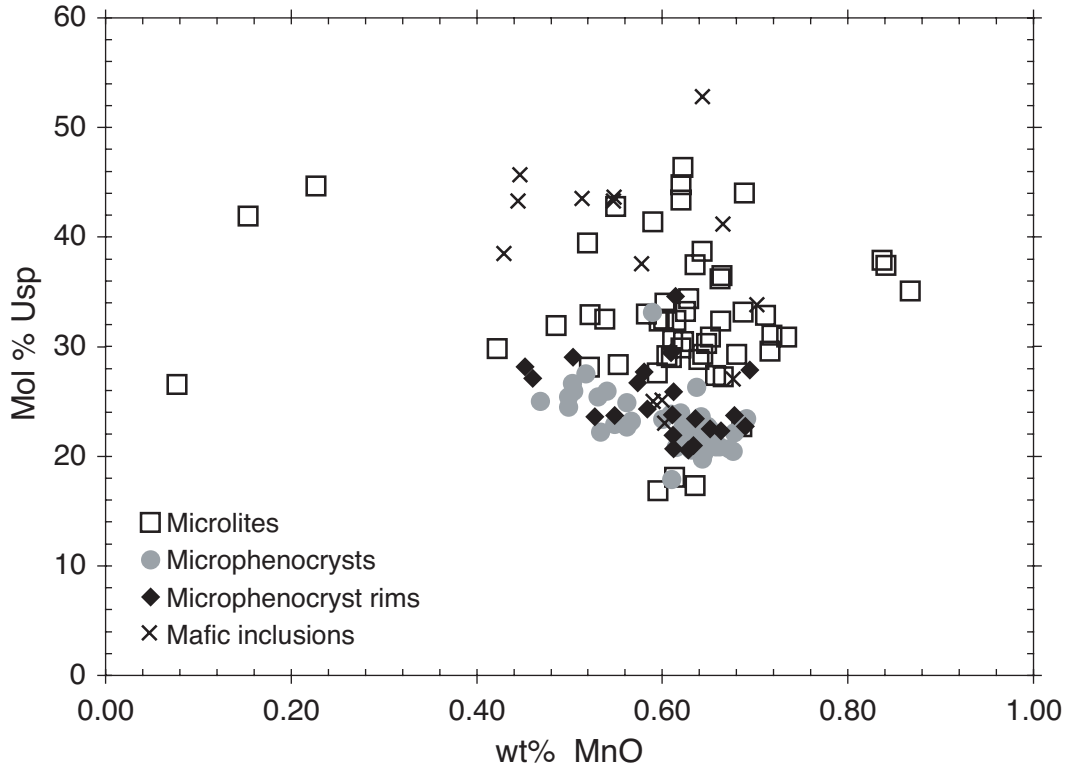


Figure 6

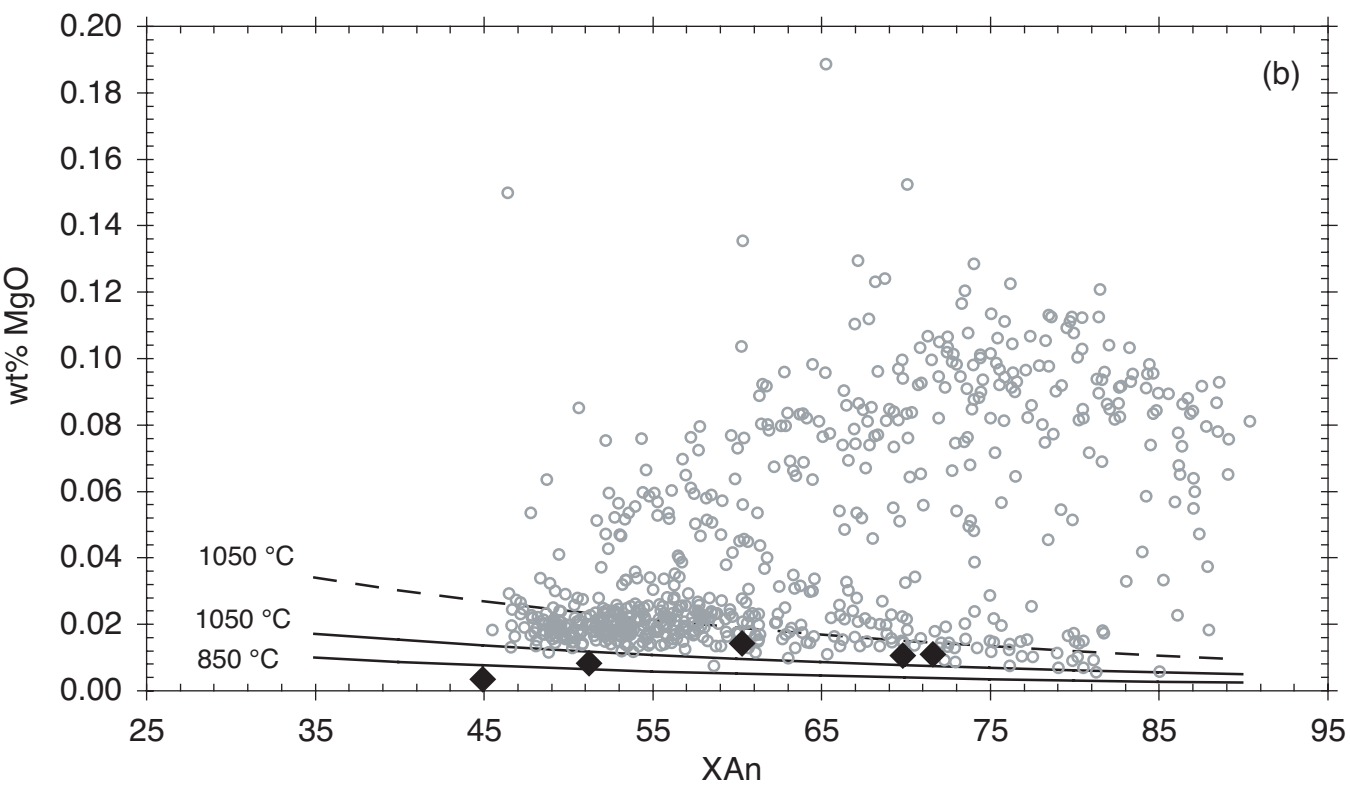
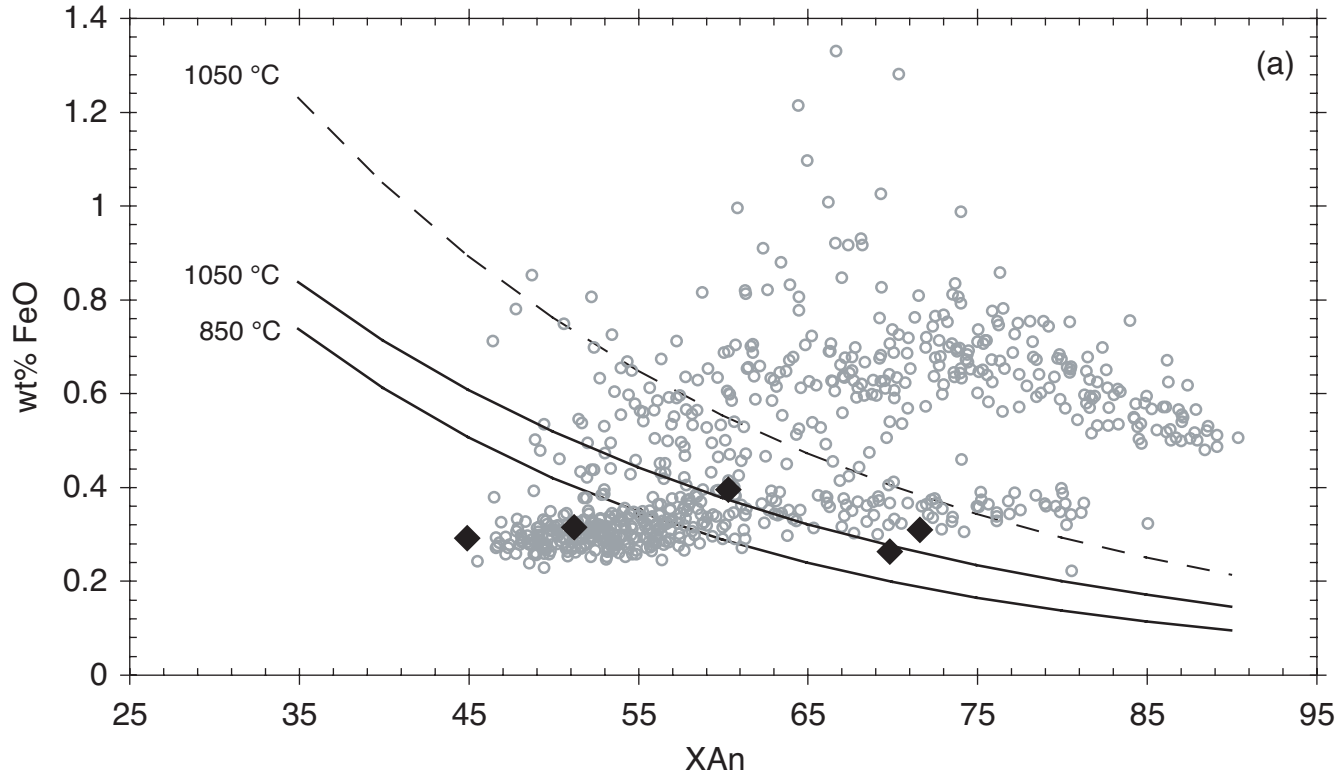


Figure 8

